

A Two-DOF Bipedal Robot Utilizing the Reuleaux Triangle Drive Mechanism

Jiteng Yang, Wael Saab, and Pinhas Ben-Tzvi, *Senior Member, IEEE*

Abstract— This paper presents the design, modeling, analysis, and experimental results of a bipedal robotic system that utilizes two interconnected single degree-of-freedom leg mechanisms to produce stable forward locomotion and steering. The legs are composed of double four-bar mechanism connected in series that maintain a parallel orientation of a flat foot, relative to the biped body, that is actuated via a Reuleaux triangle cam-follower system to produce a desirable foot trajectory. The mechanical design of the leg mechanism is presented followed by kinematic analysis of the cam-follower system to select the optimal foot trajectory and synthesize the mechanism dimensions and produce a desired step height and step length. The concept of leg sequencing is then presented to maintain a constant body height above the ground and a constant forward walking velocity. Experimental results using an integrated prototype indicate that the proposed biped robot is capable of maintaining quasi-static stability during locomotion, maintaining a constant robot body height, maintaining a constant body orientation, move forward with a constant maximum velocity of 27.4 cm/s, and steer.

I. INTRODUCTION

In recent years, the field of multi-legged robotics has drawn interests among researchers due to high levels of locomotion adaptability on the unstructured terrain. Conventional robotic leg designs consist of many active degrees-of-freedom (DOF) that enhance locomotion and tasking abilities [1]. However, each additional DOF will increase overall weight, energy consumption, and complexity of the control algorithms to simultaneously provide propulsion, stabilization, and maneuvering [2]. As a result, only a few legged robots have been successfully implemented in real-world applications. Such examples include, but are not limited to, the ANYmal quadruped [3], and Adaptive Suspension Vehicle [4].

The majority of existing legged robots are bio-inspired from animals that have evolved to adapt to their natural habitat. These robots utilize multiple DOFs to position their (primarily) single point of contact foot. The conventional walking machine uses three DOFs for each leg [5], [6]. Traditionally, one DOF is allocated to hip abduction/adduction to enable turning and is separated from the hip and knee extension/flexion mechanism that constitutes the two remaining DOFs to enable planar walking. Therefore, a $2n$ - legged robot requires $6n$ actuators, where n is the number of leg pairs. If flat feet are implemented, a more stable gait can be performed due to a larger support polygon; however, additional DOFs are needed to control the angular

orientation of the foot.

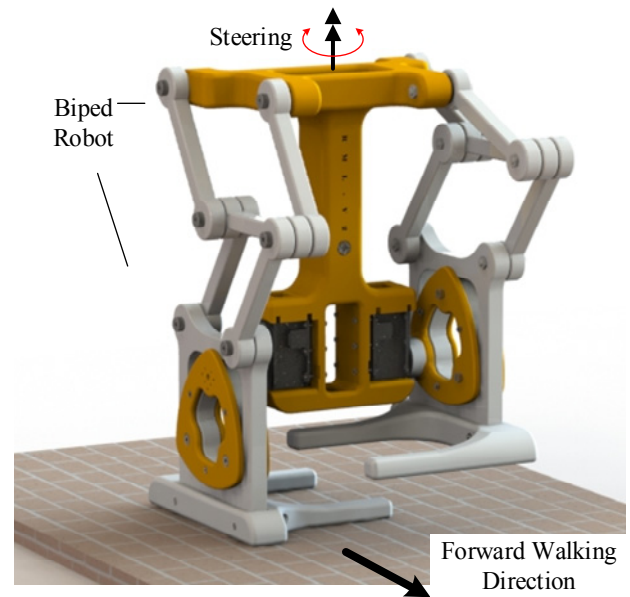


Figure 1. Design concept of biped robot constructed with two RML-V2 mechanisms.

To address the challenges of highly articulated legs, researchers have proposed reduced DOF leg designs that utilize two or less active DOFs. However, reduced articulation is coupled to reduced tasking abilities such as maintaining a constant robot body height or orientation during a walking gait [7]. The first-generation Robotic Modular Leg is a two-DOF leg proposed for the construction of both a quadruped and biped robot. The mechanism layout provided decoupled actuation for simplified control and was capable of orientating a flat foot utilizing the kinematics of a double four-bar mechanism connected in series [8], [9]. Torige et. al. [10] developed a centipede-like robot consisting of six segments, each utilizing four motors to control two legs. Hoffman et. al. [11] further developed this concept by utilizing two passive revolute joints to couple the motion between two legs. Therefore, the two legs in each can be controlled by two linear actuators to extend the body, raise the legs, and drive the robot forward. The RHex hexapod robot utilized six continuously rotating C-shaped legs to drive the robot forward with steering enabled via differential drive [12]. Yoneda et al. [13] designed a quadruped robot with three active DOF's. The robot consisted of a front and rear section that can rotate about the orientation of the robot. The roll of each segment, coupled with rotation of U-shaped front and rear legs, caused the robot to move forward. Furthermore, single-DOF crank driven mechanisms [5], [14]–[18], and

*This material is based on work supported by the National Science Foundation under Grants No. 1557312 and 1906727.

J. Yang, W. Saab and P. Ben-Tzvi are with the Robotics and Mechatronics Lab, Virginia Tech, Blacksburg, VA 24060 USA (email: {jyt,waelsaab,bentzvi}@vt.edu)

two-DOF legs that generate approximate straight line support phase foot trajectories [19], [20] have been proposed for the construction of legged robots for simplified control and design complexity.

In this paper, we propose a bipedal robot design, shown in Fig. 1, that is composed of two second-generation Robotic Modular Leg Mechanisms (RML-V2), each utilizing a single-DOF continuous rotation Reuleux triangle that are designed to generate a desired foot trajectory that enable stable forward locomotion and steering via differential drive. The first generation design [8], [9] required simultaneous control of each leg's two active DOF's to produce a desired foot trajectory that required motor directional changes which limited the maximum forward walking velocity to 10 cm/s.

The contributions of this work include the novel implementation of the Reuleux triangle cam-follower system to actuate a robotic leg mechanism. Contrary to prior applications that are concerned with motion of the Reuleux triangle in a fixed conjugate square, the proposed application requires rotation of the Reuleux triangle about an offset distance from its centroid to create translational motion of its conjugate square. The angular orientation of the conjugate square is constrained via the kinematics of two four-bar mechanisms connected in series that maintain its orientation without the use of an additional ankle motor and can therefore be used in conjunction with a flat foot support polygon to enable a quasi-static walking gait. In addition, we present the analytical formulations describing the trajectory of the conjugate square centroid as a function of a rotational offset from the Reuleux triangle centroid. These formulations are further analyzed to produce a desirable foot trajectory for a walking gait to synthesize Reuleux triangle dimensions and its angular rotation to generate a foot trajectory of desired step height and length while maintaining a constant forward walking velocity during the support phase.

II. DESIGN MOTIVATION

Although reduced-DOF leg mechanisms do enable the construction of legged robots with reduced design and control complexity; the reduced articulation may hinder the robot's walking performance. For instance, the Rhex robot [12] and 3-DOF quadruped [13] are capable of walking forward, but the robot's body height and orientation fluctuate during a walking gait. Such characteristics are undesirable since they may induce instances of instability and require additional energy to raise the body vertically against gravity. Therefore, we design the robotic system to satisfy five necessary walking functionalities, as presented in [7]. These functionalities are listed as follows: (1) maintain quasi-static stability during locomotion, (2) maintain a constant robot body height during a waiting gait, (3) maintain a constant body orientation during a walking gait, (4) move forward, and (5) steer.

Criteria (1) and (2) are required to maintain a stable robotic platform in static configurations and during a walking gait, in addition to improving the energy efficiency of the system since the legs will not be required to raise or lower the body cyclically. Criterion (3) ensures a sufficient margin of stability within the support polygon defined as the center-of-mass projection into the convex hull of the robot's feet in contact with the ground. Criteria (4) and (5) ensure the

sufficient amount of locomotion capabilities to enable the robot to move forward and be steered in any desired position and direction.

III. ROBOTIC MODULAR LEG – V2

This section reviews prior research into the design, and implementation of the Reuleux triangle (section 2.1) that represents the main driving mechanism of the RML-V2 design (section 2.2). Kinematic analysis is presented (section 2.3) to formulate the analytical expressions describing the foot trajectory and synthesize the Reuleux triangle dimensions to produce a desired step height and length.

A. Background

In the work by Leonardo da Vinci circa 1514, the map of earth was projected onto a circle using eight pairs of triangular-shaped octants. The special properties of this shape, consisting of an equilateral triangle with curved sides to maintain an equal distance from any vertex to its opposing periphery, was later defined by Franz Reuleux in 1876. In his book [21], a qualitative study demonstrated how this mechanism can be used as a function generator. Thus, leading to the first major industrial application of the Reuleux triangle, to construct the Wankel internal combustion engine, which rotated within an epitrochoidal confinement to produce suitable changing gas volumes in three chambers. James Watts then proposed to rotate the Reuleux triangle within a conjugate square profile and place cutting tools at each vertex to drill square-shaped holes [22]. This application was later studied by Figliolini et al. who presented the analytical expressions describing the motion of particular points on the Reuleux triangle during its rotation within a fixed conjugate square [23].

B. Mechanical Design

Fig. 2 shows a side view schematic diagram of the RML-V2. The leg is composed of double four-bar mechanism parallelograms connected in series that comprise the thigh and shin that rotate about the hip and knee joints, respectively. Therefore, the orientation of the foot maintains a constant angular orientation with respect to the body without the need for an additional motor at the ankle. The RML-V2 is actuated with an active single-DOF in the form of a Reuleux triangle cam-follower system. In this case, the cam is the Reuleux triangle and the follower is the conjugate square shaped foot. As opposed to previous applications, the Reuleux triangle is rotated at an offset from its centroid to produce a desirable foot trajectory while the foot maintains a constant orientation due to the coupled four-bar mechanism as will be discussed in section 4.

Comparing to the first generation RML [8], [9], these design features represent an improvement over the first generation. The first generation RML has two active DOFs, thus, in order to achieve locomotion, two active DOFs need to be synchronized therefore increase the complexity in the control of the robot. The RML-V2, however, utilizes single active DOF to achieve locomotion. Hence, the control strategy simplified. Furthermore, the continuous rotation of a single motor will produce a forward walking gait that can result in potentially higher walking velocities as will be presented in subsequent sections.

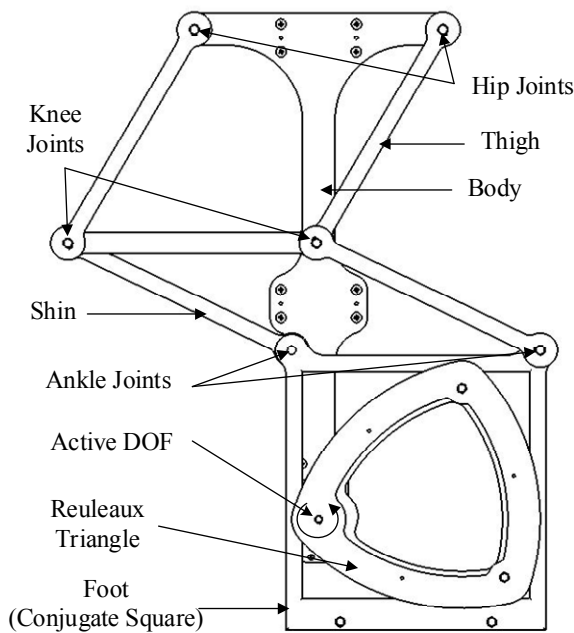


Figure 2. Side view schematic diagram of the RML-V2.

C. Kinematic Analysis

This section presents the kinematic analysis of Reuleaux triangle (cam) and its foot follower (conjugate square). Prior applications [22], and analysis [23] were concerned with the motion of the Reuleaux triangle within a stationary conjugate square. We build upon previous work by formulating the analytical expressions resulting from rotation of the Reuleaux triangle about an offset distance from its centroid to produce a desirable conjugate square centroid trajectory, while maintaining a fixed orientation (discussed in section 3.2), and synthesize the mechanism dimensions to produce a desirable step length and height.

Fig. 3 shows the schematic diagram of the Reuleaux triangle driving mechanism of the RML-V2 that is used to construct the biped robot. The triangle is composed of an equilateral triangle of side length l with three vertices U , V , W , and rotates within a conjugate square with corners defined as H , I , J , K . Let G represent the centroid location of the conjugate square. To ensure functionality of the driving mechanism, the Reuleaux triangle contours and conjugate square must have a radius of curvature and length equivalent to l [21]. A body-attached frame of reference (B , \mathbf{i}_1 , \mathbf{i}_2) is attached to Reuleaux triangle at its centroid B . The Reuleaux triangle rotates about point O with an input angle α . Point O is offset from the centroid B by a distance $|\rho|$ along \mathbf{i}_1 . The Reuleaux triangle and its conjugate square form a single DOF system where rotation of the triangle results in a planar displacement of the conjugate square in the inertial frame (I , \mathbf{x} , \mathbf{y}).

The notation $\mathbf{p}_j^{(i)}$ will be used to represent the position of point j in frame i . Furthermore, the scalar x - and y -components of an arbitrary vector Z will be represented as Z_x and Z_y respectively

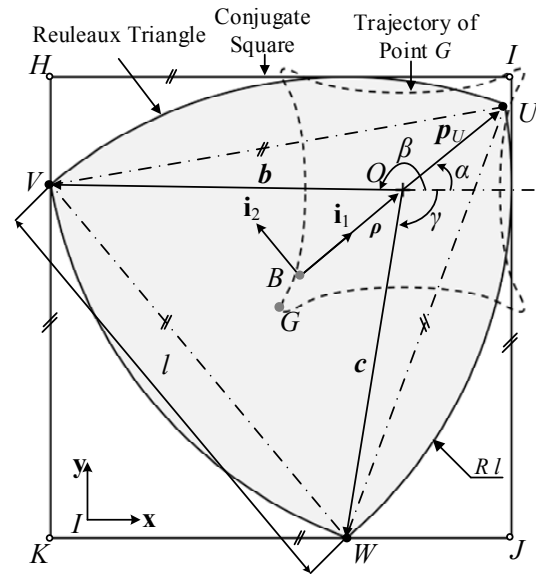


Figure 3. Schematic of Reuleaux triangle and its conjugate square.

Referring to Fig. 3, the position of conjugate square centroid $\mathbf{p}_G^{(I)}$ is given by (1) that computes the G_x and G_y component of the position vector $\mathbf{p}_G^{(I)}$ in the global reference frame based on the contact point of each vertex with the sides of the conjugate square, dependent on the input angle rotation.

As seen in (1), $\mathbf{p}_G^{(I)}$ needs only to be computed for the input angle $\alpha = [0, \pi/2]$ while the remaining trajectory profile may be generated with symmetry operations due to the geometric symmetry of the Reuleaux triangle.

$$\mathbf{p}_G^{(I)} = \begin{cases} \left(Ux - \frac{l}{2} \right) \mathbf{x} + \left(Wy + \frac{l}{2} \right) \mathbf{y}, \alpha = [0, \frac{\pi}{6}) \\ \left(Vx + \frac{l}{2} \right) \mathbf{x} + \left(Wy + \frac{l}{2} \right) \mathbf{y}, \alpha = [\frac{\pi}{6}, \frac{\pi}{3}) \\ \left(Vx + \frac{l}{2} \right) \mathbf{x} + \left(Uy - \frac{l}{2} \right) \mathbf{y}, \alpha = [\frac{\pi}{3}, \frac{\pi}{2}] \end{cases} \quad (1)$$

However to evaluate (1), the vertex positions of the Reuleaux triangle defined as $\mathbf{p}_U^{(I)}$, $\mathbf{p}_V^{(I)}$ and $\mathbf{p}_W^{(I)}$ can be computed by coordinate transformation from B to I using following equations:

$$\begin{aligned} \mathbf{p}_U^{(I)} &= \mathbf{T}_B^I(\alpha)(-\rho^{(B)} + \mathbf{p}_U^{(B)}) + \mathbf{p}_O^{(I)} \\ \mathbf{p}_V^{(I)} &= \mathbf{T}_B^I(\alpha)(-\rho^{(B)} + \mathbf{p}_V^{(B)}) + \mathbf{p}_O^{(I)} \\ \mathbf{p}_W^{(I)} &= \mathbf{T}_B^I(\alpha)(-\rho^{(B)} + \mathbf{p}_W^{(B)}) + \mathbf{p}_O^{(I)} \end{aligned} \quad (2)$$

Here, $\mathbf{T}_B^I(\alpha)$ represents the rotation matrix from frame B to I for an input angle of α . The vertices and rotational offset in the body fixed frame B are defined as

$$\begin{aligned} \mathbf{p}_U^{(B)} &= \frac{l}{\sqrt{3}} \mathbf{i}_1, \mathbf{p}_V^{(B)} = -\frac{l}{2\sqrt{3}} \mathbf{i}_1 + \frac{l}{2} \mathbf{i}_2 \\ \mathbf{p}_W^{(B)} &= -\frac{l}{2\sqrt{3}} \mathbf{i}_1 - \frac{l}{2} \mathbf{i}_2, \rho^{(B)} = \rho \mathbf{i}_1 \end{aligned} \quad (3)$$

Conjugate square trajectory: With reference to Appendix A, the trajectory of point G , denoted as π_1 for various offset values ρ , are illustrated in Fig. 4. The profiles are normalized with respect to the triangle length l where $\alpha=[0, 2\pi]$. It is interesting to note that trajectory profile varies with respect to different offset of ρ . $\pi_1, \pi_2, \pi_3, \pi_4$, and π_8 are shown in Fig. 4(A). $\rho=|BU|$ yields π_1 , a straight sided quadrilateral profile. When $0.5(l-|BU|)<\rho<|BU|$, the trajectory profiles represent a concaved sided quadrilateral. For $\rho=0.5(l-|BU|)$ the trajectory denoted as a superellipse or Lamé curve [21].

Fig. 4(B) illustrates trajectories π_5, π_6 , and π_7 on a magnified scale of factor 3. For $(|BU|-l/2)<\rho<0.5(l-|BU|)$ the trajectory π_5 resembles a profile with four concave elliptical curves that intersect with its neighboring curves and form loops. Similarly for $\rho=(|BU|-l/2)$ the π_6 trajectory loop curves are tangent to one another forming what is referred to as a homocentral form of π_5 . For $0<\rho<(|BU|-l/2)$ the π_7 trajectory forms four elliptical curves that intersect with each other. For $\rho=0$, the π_8 trajectory forms a profile with four convex elliptical curves that are tangent to neighboring curves [21].

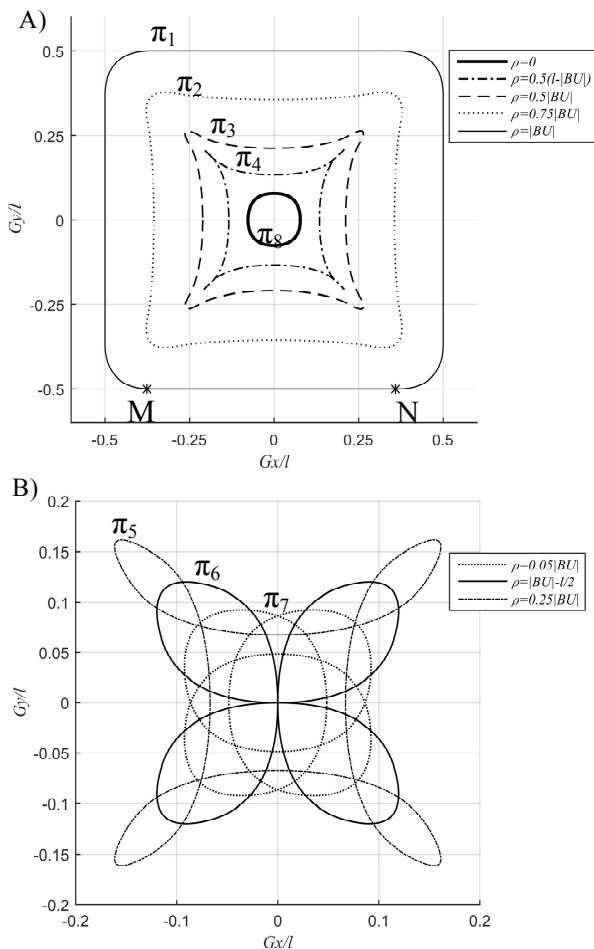


Figure 4. Trajectory profiles of point G normalized with respect to l for various offset values ρ .

IV. FOOT TRAJECTORY PLANNING

The trajectory planning involves finding optimal ρ to obtain a straight line support phase and gait sequencing such that the robot could maintain constant bodyheight and

walking speed during locomotion. The support phase is defined as the foot trajectory portion that is in contact with the ground, while the swing phase involves swinging the foot in mid-air. As discussed in section 2, it is desirable to maintain a constant robot body height and orientation to minimize energy consumption during a forward walking gait. Therefore, a straight line support phase is desirable to satisfy these conditions.

Referring to Fig. 4(A), π_1 illustrates a straight sided quadrilateral. Therefore, the rotational offset distance from the Reuleaux triangle centroid should be set to $\rho = |BU|=l/\sqrt{3}$ to generate this foot trajectory.

Let step stroke length and step height be defined as the maximum range of horizontal and vertical distance of the trajectory profile, respectively. The distance between points M and N on the π_1 trajectory defines the step length that will be used to propel the robot forward which is slightly shorter than the step stroke length.

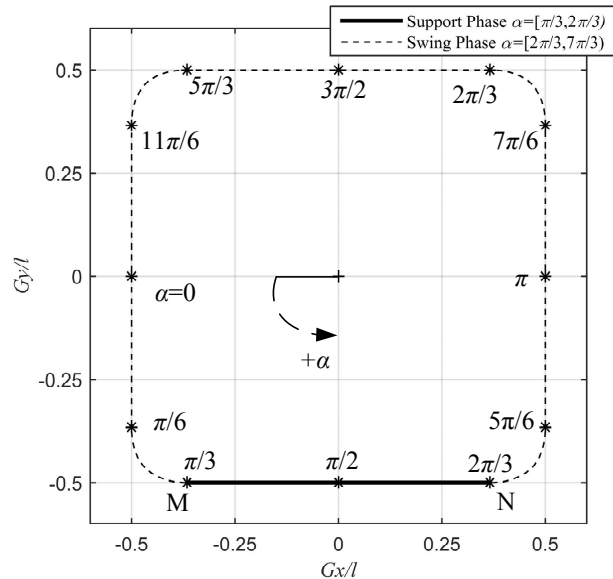


Figure 5. Foot trajectory profile with input angle α .

With reference to Appendix A and Fig. 5, and due to the symmetric about x and y axis; the step height and step stroke yields l .

It can also be noticed that in Fig. 5, the support phase of the robot initiates when $\alpha = \pi/3$ and terminates when $\alpha = 2\pi/3$. Substituting these values into (8) (Appendix A) yields the coordinate of point M and point N. Therefore, the step length is equivalent to $l(\sqrt{3} - 1)$.

A. Gait Sequencing

This section will analyze the requirements of the input angle α trajectory to maintain constant walking velocity during the support phase while maintaining constant body height for $\rho=|BU|$. As mention in section 4, the foot trajectory π_1 is selected for a straight line support phase to ensure a constant body height and the legs of the biped are sequenced such that the one leg initiates the support phase while the other leg must simultaneously initiate the swing phase, and vice versa. Otherwise, the robot body will fluctuate vertically and may cause instances of instability. Furthermore, it is

desirable to have a constant forward walking velocity, v , during a walking gait to avoid variations in acceleration that may induce instances of instability.

With reference to Fig. 5, the gait cycle period is obtained by the summation of time for support and swing phase. In this work, the support phase time is equal to the swing phase time, The gait cycle period, for a combined single swing and single support phase, can be obtained by (4)

$$T = 2 \frac{MN}{v} = \frac{l}{v} (2\sqrt{3} - 2) \quad (4)$$

The walking velocity of the robot can also be obtained by the time derivative of $\mathbf{p}_G^{(I)}$. With reference to Appendix A, the time derivative of (8) for $\pi/3 \leq \alpha \leq \pi/2$ yields the horizontal velocity of the conjugate square for half the support phase:

$$-\frac{d\alpha}{dt} \frac{l}{2} \cos(\alpha) + \frac{d\alpha}{dt} \frac{\sqrt{3}}{2} l \sin(\alpha) = v \quad (5)$$

We define $\tau = t/T$ to be the percentage of a gait cycle. Let $\tau_{\text{support}} = 1/2$ be defined as the duty cycle, solving (5) yields the trajectory of α , (6) and (7) for $\pi/3 \leq \alpha < \pi/2$ and $\pi/2 \leq \alpha \leq 2\pi/3$, respectively:

$$\alpha = \arcsin\left((2\sqrt{3} - 2)\tau - C_1\right) + \frac{2\pi}{3}, \alpha \in \left[\frac{\pi}{3}, \frac{\pi}{2}\right] \quad (6)$$

$$\alpha = \arcsin\left((2\sqrt{3} - 2)\tau - C_2\right) + \frac{\pi}{3}, \alpha \in \left[\frac{\pi}{2}, \frac{2\pi}{3}\right] \quad (7)$$

Here, C_1 and C_2 are integral constants which can be obtained by initial conditions.

To achieve a smooth transition from support phase to swing phase, quintic splines are used to generate the rotation angle trajectory for swing phase.

V. EXPERIMENT RESULTS

This section presents prototype integration (section 5.1), and demonstrates walking capabilities of the biped robot (section 5.2).

A. Prototype Integration

The prototype measures 230 x 200 x 320 mm and weights 2.5 kgs. The Reuluex triangle dimensions were selected to produce a gait cycle designed step height and length equivalent to 75 mm and 54.9 mm, respectively. The

prototype is fixed to a stable surface to measure the actual foot trajectory. The actual foot trajectory was tracked utilizing computer vision method by tracking a blue marker on attached to the conjugate square foot. The actual foot trajectory and theoretical trajectory are presented in Fig. 6. The actual foot trajectory is presented as dashed line and theoretical trajectory is presented as solid line.

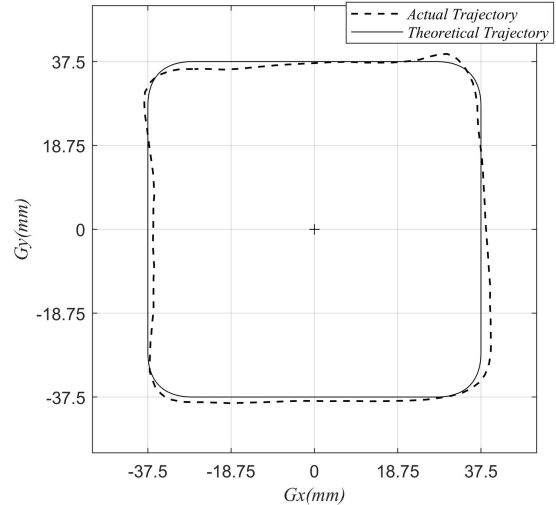


Figure 6. Experimental and calculated foot trajectory.

Further analysis indicates that the overall average error of x coordinate is 0 with standard deviation of 0.86 and the overall average error of y coordinate is 0.03 with standard deviation of 0.82. It can also be noticed in the figure that the for the support phase, the theoretical and actual foot trajectory coincides, therefore, it can be safely assumed that the actual support phase of the prototype is a straight line.

B. Walking Capabilities

To evaluate the walking conditions of the biped, the robot was commanded to walk forward, Fig. 7(A-F), and turn, Fig. 7(G-L), using differential drive where one foot maintains a support phase while the opposing foot produces a cyclic gait cycle. Fig. 8 shows the x and y displacement of the robot during walking. It can be noticed that in Fig. 8 the body maintained a constant height and walking with constant velocity of 21mm/s. For turning capabilities, a single gait cycle resulted 18° of turning.

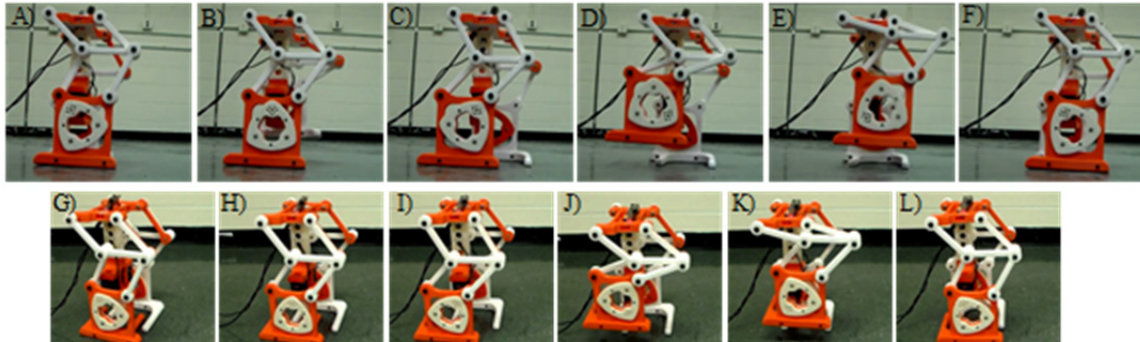


Figure 7. Biped robot demonstrating forward locomotion (A-F), and differential turning (G-L).

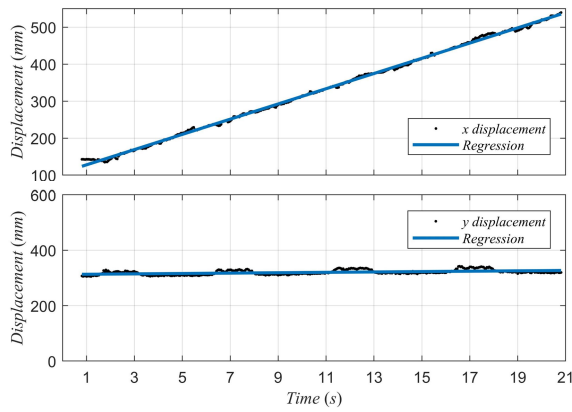


Figure 8. Prototype x and y displacement during straight walking

As demonstrated in these experiments the biped robot, composed of two single-DOF RML-V2 mechanisms, is capable of satisfying all the walking criteria discussed in section 2. The robot is capable of maintaining quasi-static stability during locomotion, maintaining a constant robot body height during a waiting gait, maintaining a constant body orientation during a walking gait, move forward, and steer.

VI. CONCLUSION

This paper presented a conceptual design and implementation of a classical mechanism called the Reuleaux triangle that is connected to a double four bar mechanism. The kinematics of the mechanism were derived to select a rotational offset distance from the Reuleaux triangle centroid to produce a straight line support phase with a constant robot body height and forward walking velocity. Experimental results of the bipedal robot demonstrated the walking capabilities where the robot can produce a quasi-static forward walking gait and turning while maintaining a constant velocity, body height and orientation.

APPENDIX

Due to the symmetry of the mechanism, only the conjugate square centroid trajectory for an input angle $\alpha = [0, \pi/2]$ needs to be calculated. The trajectory of the conjugate square yields (8).

$$p_G^{(l)} = \begin{cases} \left[\left(\frac{l}{\sqrt{3}} - \rho \right) \cos(\alpha) - \frac{l}{2} \right] x + \left[-\frac{1}{6}(\sqrt{3}l + 6\rho) \sin(\alpha) + \frac{l}{2}(1 - \cos(\alpha)) \right] y, \alpha = [0, \frac{\pi}{6}] \\ \left[\frac{l}{2}(1 - \sin(\alpha)) - \frac{1}{6}(\sqrt{3}l + 6\rho) \cos(\alpha) \right] x + \left[-\frac{1}{6}(\sqrt{3}l + 6\rho) \sin(\alpha) + \frac{l}{2}(1 - \cos(\alpha)) \right] y, \alpha = [\frac{\pi}{6}, \frac{\pi}{3}] \\ \left[\frac{l}{2}(1 - \sin(\alpha)) - \frac{1}{6}(\sqrt{3}l + 6\rho) \cos(\alpha) \right] x + \left[\left(\frac{l}{\sqrt{3}} - \rho \right) \sin(\alpha) - \frac{l}{2} \right] y, \alpha = [\frac{\pi}{3}, \frac{\pi}{2}] \end{cases} \quad (8)$$

REFERENCES

- [1] M. F. Silva and J. A. T. MacHado, "A historical perspective of legged robots," *JVC/Journal Vib. Control*, vol. 13, no. 9–10, pp. 1447–1486, 2007.
- [2] J. A. Galvez, J. Estremera, and P. G. De Santos, "A new legged-robot configuration for research in force distribution," *Mechatronics*, vol. 13, no. 8, pp. 907–932, 2003.
- [3] M. Hutter *et al.*, "ANYmal - A highly mobile and dynamic quadrupedal robot," in *IEEE International Conference on Intelligent Robots and Systems*, 2016, vol. 2016-Novem, pp. 38–44.
- [4] K. J. Waldron and R. B. McGhee, "The Adaptive Suspension Vehicle,"

- IEEE Control Syst. Mag.*, vol. 6, no. 6, pp. 7–12, 1986.
- [5] M. Kaneko, M. Abe, K. Tanie, S. Tachi, and S. Nishizawa, "Basic Experiments on a Hexapod Walking Machine (MELWALK-III) with an Approximate Straight-Line Link Mechanism," in *1985 International Conference on Advanced Robotics*, 1985, pp. 397–404.
- [6] G. M. Nelson and R. D. Quinn, "Posture control of a cockroach-like robot," in *Proceedings - IEEE International Conference on Robotics and Automation*, 1998, vol. 1, pp. 157–162.
- [7] M. Kaneko, M. Abe, S. Tachi, S. Nishizawa, K. Tanie, and K. Komoriya, "Legged Locomotion Machine Based on the Consideration of Degrees of Freedom," *Theory Pract. Robot. Manip.*, pp. 403–410, 2012.
- [8] W. Saab and P. Ben-Tzvi, "Design and Analysis of a Robotic Modular Leg Mechanism," 2016, International Design Engineering Technical Conferences and Computers and Information in Engineering Conference, Volume 5A: *40th Mechanisms and Robotics Conference* p. V05AT07A062, doi:10.1115/DETC2016-59388.
- [9] W. Saab, W. S. Rone, and P. Ben-Tzvi, "Robotic Modular Leg: Design, Analysis, and Experimentation," *J. Mech. Robot.*, vol. 9, no. 2, pp. 024501–024506, 2017.
- [10] A. Torige, M. Noguchi, and N. Ishizawa, "Centipede type multi-legged walking robot," in *Proceedings of 1993 IEEE/RSJ International Conference on Intelligent Robots and Systems (IROS '93)*, 2002, pp. 567–571.
- [11] K. L. Hoffman and R. J. Wood, "Passive undulatory gaits enhance walking in a myriapod millirobot," in *IEEE International Conference on Intelligent Robots and Systems*, 2011, pp. 1479–1486.
- [12] U. Saranlı, M. Buehler, and D. E. Koditschek, "RHex: A simple and highly mobile hexapod robot," *Int. J. Rob. Res.*, vol. 20, no. 7, pp. 616–631, 2001.
- [13] K. Yoneda, Y. Ota, F. Ito, and S. Hirose, "Construction of a quadruped with reduced degrees of freedom," in *IECON Proceedings (Industrial Electronics Conference)*, 2000, vol. 1, pp. 28–33.
- [14] H. Funabashi, K. Ogawa, Y. Gotoh, and F. Kojima, "Synthesis of Leg-Mechanisms of Biped Walking Machines : Part I, Synthesis of Ankle-Path-Generator," *Bull. JSME*, vol. 28, no. 237, pp. 537–543, 2011.
- [15] C. Liang, M. Ceccarelli, and Y. Takeda, "Operation Analysis of a One-DOF Pantograph Leg Mechanisms," in *Proceedings of the RAAD 2008*, 2008, pp. 1–10.
- [16] N. G. Lokhande and V. B. Emche, "Mechanical Spider by Using Klann Mechanism," *Int. J. Mech. Eng. Comput. Appl.*, vol. 1, no. 5, pp. 13–16, 2013.
- [17] C. Tavorlieri, E. Ottaviano, M. Ceccarelli, and A. Di Rienzo, "Analysis and Design of a 1-DOF Leg for Walking Machines," in *Mediterranean Conference on Control and Automation*, 2007, pp. 15–17.
- [18] V. R. Kamidi, W. Saab, and P. Ben-Tzvi, "Design and analysis of a novel planar robotic leg for high-speed locomotion," in *IEEE International Conference on Intelligent Robots and Systems*, 2017, vol. 2017-Septe, pp. 6343–6348.
- [19] H. Adachi, N. Koyachi, and E. Nakano, "Mechanism and Control of a Quadruped Walking Robot," *IEEE Control Syst. Mag.*, vol. 8, no. 5, pp. 14–19, 1988.
- [20] L. E. Ch., P. C., P. F., and D. V., "Novel Solution for Leg Motion with 5-Link Belt Mechanism," *Int. J. Appl. Mech. Eng.*, vol. 19, no. 4, pp. 699–708, 2015.
- [21] F. Reuleaux, *Kinematics of machinery: outlines of a theory of machines*. Courier Corporation, 2012.
- [22] Harry J Watts, "Drill or boring member," US1241176A, 1917.
- [23] G. Figliolini, P. Rea, and S. Grande, "Higher-Pair Reuleaux-Triangle in Square and its Derived Mechanisms," in *ASME 2012 International Design Engineering Technical Conferences and Computers and Information in Engineering Conference*, 2013, pp. 1629–1638.